Soft Matter

PAPER

View Article Online
View Journal | View Issue

Cite this: *Soft Matter*, 2014, **10**, 2388

Oscillations of Min-proteins in micropatterned environments: a three-dimensional particle-based stochastic simulation approach†

Max Hoffmann[ab] and Ulrich S. Schwarz*[ab]

Received 22nd August 2013
Accepted 29th October 2013

DOI: 10.1039/c3sm52251b

www.rsc.org/softmatter

The Min-proteins from *E. coli* and other bacteria are the best characterized pattern forming system in cells and their spatiotemporal oscillations have been successfully reconstituted *in vitro*. Different mathematical and computational models have been used to better understand these oscillations. Here we use particle-based stochastic simulations to study Min-oscillations in patterned environments. We simulate a rectangular box of length 10 μm and width 5 μm that is filled with grid or checkerboard patterns of different patch sizes and distances. For this geometry, we find different stable oscillation patterns, typically pole-to-pole oscillations along the minor axis and striped oscillations along the major axis. The Min-oscillations can switch from one pattern to the other, either effected by changes in pattern geometry or stochastically. By automatic analysis of large-scale computer simulations, we show quantitatively how the perturbing effect of increased patch distance can be rescued by increased patch size. We also show that striped oscillations occur robustly in arbitrarily shaped filamentous *E. coli* cells. Our results highlight the robustness and variability of Min-oscillations, put limits on the effect of putative division sites, and provide a powerful computational framework for future studies of protein self-organization in patterned environments.

1 Introduction

Min-proteins allow bacteria like *E. coli* to find the middle at which to divide in order to effect two equally sized daughter cells.[1] In 1999, it was found that this mechanism is in fact based on a spatiotemporal oscillation[2] which since then has emerged as the best studied example of a protein pattern forming system in cells. At the core of this system are only two proteins, MinD and MinE. MinD is an ATPase that binds to the bacterial membrane after loading with ATP. There it recruits MinE, which accelerates hydrolysis and thus leads to release of MinD. The released MinD can be loaded again with ATP and rebinds at a new location, thus providing the basic mechanism for wave propagation along the membrane. A third Min-protein, MinC, is not necessary for the oscillations, but follows the MinD pattern.[3,4] In wildtype cells, MinD sequentially localizes to one pole after the other (pole-to-pole oscillation), with MinE forming a ring at the rim of the retracting polar zones. On average, this keeps MinD and thus also MinC away from the middle of the cell. This in turn allows the assembly of a FtsZ-ring in the middle and eventually leads to symmetric cell division.[5] The details of the Min-system have been extensively reviewed elsewhere,[6–8] but there remain some open issues. For example, it has been suggested that cytoplasmic diffusion of the Min-proteins is not relevant and that there exist additional protein interactions at the membrane which lead to very specific local wave structures.[9]

One of the most striking features of the Min-system is that stable oscillations also occur in other geometries than the wildtype cell. A typical *E. coli* wildtype cell has a length of 2–5 μm and a width of 0.5–2 μm and the oscillation period is typically around 1 min.[2] During growth the length approximately doubles. Already before the septum closes, stable oscillations emerge in the two daughter cells.[10] However, if division is suppressed by FtsZ-depletion, one obtains very long (*filamentous*) cells in which the oscillation pattern changes from pole-to-pole (with the two localization regions at the poles) to striped (with more than two localization regions distributed along the whole length in a stripe-like manner), with a characteristic distance between adjacent localization regions of 5 μm^2. It has also been shown that in *E. coli* mutants with a Y-shape, different oscillation patterns can arise depending on the actual arm lengths.[11] In spherical cells no stable oscillation patterns have been observed. Rather in this case MinD moves to and from multiple sites on the cell surface.[12] In irregularly shaped *E. coli* cells obtained by squeezing the cells in nano-channels,

[a]*BioQuant, Heidelberg University, Im Neuenheimer Feld 267, 69120 Heidelberg, Germany. E-mail: ulrich.schwarz@bioquant.uni-heidelberg.de; Fax: +49 6221 54 51482; Tel: +49 6221 54 51254*

[b]*Institute for Theoretical Physics, Heidelberg University, Philosophenweg 19, 69120 Heidelberg, Germany*

† Electronic supplementary information (ESI) available: Three movies and eleven additional figures. See DOI: 10.1039/c3sm52251b

oscillations have been observed, however, the oscillation axis is not well defined.[13] Thus the spatiotemporal details of the Min-oscillations strongly depend on the membrane geometry.

Recently, it has been demonstrated that Min-oscillations can be reconstituted *in vitro* using supported bilayers.[14,15] On these homogeneous flat substrates, spiral and stripe patterns are found, on a length scale (50–100 μm) that is much larger than in the *in vivo* system (5 μm). By using micropatterning techniques, it was shown that these surface waves are sufficiently robust as to tolerate gaps in the substrate up to the scale of the typical pattern length scale.[16] The waves were also sufficiently robust as to tolerate the reduction of protein diffusion in the medium by up to one order of magnitude. Furthermore it was shown that the Min-waves sense the geometry of the substrate by orientating in the direction of the longest path on the pattern and following bends in lengthy substrate patterns.

A large range of mathematical and computational models has been suggested to better understand the underlying mechanisms and the role of geometry, starting right after their experimental discovery.[17–19] All models are based on a reaction-diffusion mechanism, but the details of the treatment vary widely. They can be classified in several ways. First one has to differentiate between mathematical models based on partial differential equations (PDEs) and computational models, which in turn can be classified as grid-based or particle-based. Second the models can be classified as one-,[17–19] two-[20] and three-dimensional.[21–23] Third they differ in the way the interactions between MinD, MinE and the membrane are treated. In this regard, the models can be divided into two large groups: Collaborative Attachment (CA) models and Aggregation Current (AC) models.[24] The main difference between these models is the way MinD clustering on the membrane is modeled. In the CA models it is assumed that MinD binds preferentially to already membrane-bound MinD, whereas in the AC models MinD can bind anywhere to the membrane, however it is clustered afterwards by attractive interaction between membrane-bound MinD molecules. Some of the early models made assumptions about reactions that were later shown to be inconsistent with experimental data. One influential model is the one devised by Huang and coworkers in 2003.[21] The Huang-model is a PDE-based CA model that predicts many of the known experimental results for a three-dimensional cylindrical cell. It has been adapted later to study important aspects of the Min-system in more detail, for example the exact role of flux currents (*channeling*)[20] or additional mechanisms like transient MinE binding,[16] for which experimental evidence exists.[15,25]

Here we focus on patterned environments as an exciting tool to quantitatively study important pattern forming protein systems like the Min-system. Particle-based stochastic simulations ideally complement this approach because they allow us to account for the effects of three dimensions, geometry, and stochastic fluctuations. In this paper, we especially focus on two technical challenges arising from the interplay of using particle-based stochastic simulations and micropatterns: implementing the two-dimensional patterned boundary conditions for the three-dimensional simulations and automatically analyzing data from large-scale computer simulations for a large range of different pattern geometries. Our starting point is the Huang-model, because it can be easily adapted for stochastic simulations. For example, it has been used with such an approach to study the effect of MinD-filaments[26] and the effect of stochastic fluctuations for the accuracy of midpoint determination using the software package MCell.[22] The Huang-model has also been used for grid-based simulations of Min-oscillations in spherical and filamentous cells using the software package MesoRD.[23] Here we use it to demonstrate some surprising generic phenomena arising from the interplay between geometry and stochastic fluctuations in three dimensions. In the future, this approach might be extended to more detailed models for the Min-system.

In order to explore the effect of structured patterns of a total size comparable to *E. coli* with patch sizes and distances well below the pattern length scale of the Min-oscillations in *E. coli*, we performed extensive computer simulations using the software package Smoldyn.[27,28] We found that this approach is very powerful in revealing selection of and switching between different oscillation patterns. We start with an introduction of the model and our simulation environment in Section 2. After introducing the results for a homogeneous substrate as a reference case in Section 3.1, in Sections 3.2 and 3.3 we show some striking examples of our simulations that illustrate the most important features found. A complete set of geometries is then automatically analyzed with the help of an oscillation analysis in Section 3.4. We also investigate the effect of three dimensions for filamentous cells in Section 3.5. We finally conclude with a discussion of our results.

2 Simulation setup

2.1 Reaction scheme and model parameters

In this publication we use the model originally introduced by Huang *et al.*,[21] which has later been adapted for particle-based stochastic simulations.[22,23] Similar to ref. 23 we do not consider a potential positive effect of membrane-bound MinDE on the binding of MinD–ATP. The resulting reaction scheme is shown in Fig. 1.

The reaction cycle starts with the exchange of ADP with ATP on a MinD–ADP molecule:

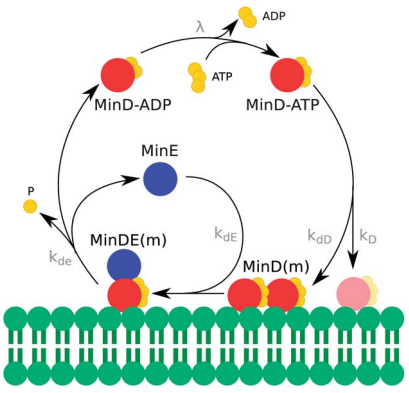

Fig. 1 Reaction scheme for the Min-oscillations. The rate constants corresponding to each reaction are marked in grey.

Table 1 Parameters used in the model. (P) denotes the reaction probability and (B) denotes the binding radius computed by Smoldyn

Parameter	Value	Value in Smoldyn
D_D	2.5 $\mu m^2\ s^{-1}$	2.5 $\mu m^2\ s^{-1}$
D_E	2.5 $\mu m^2\ s^{-1}$	2.5 $\mu m^2\ s^{-1}$
D_d	0.01 $\mu m^2\ s^{-1}$	0.01 $\mu m^2\ s^{-1}$
D_{de}	0.01 $\mu m^2\ s^{-1}$	0.01 $\mu m^2\ s^{-1}$
λ	0.5 s^{-1}	5×10^{-5} per step (P)
k_D	0.025 $\mu m\ s^{-1}$	0.00028 per step (P)
k_{dD}	0.0149 $\mu m^3\ s^{-1}$	0.0091 μm (B)
k_{dE}	0.093 $\mu m^3\ s^{-1}$	0.0179 μm (B)
k_{de}	0.7 s^{-1}	7×10^{-5} per step (P)

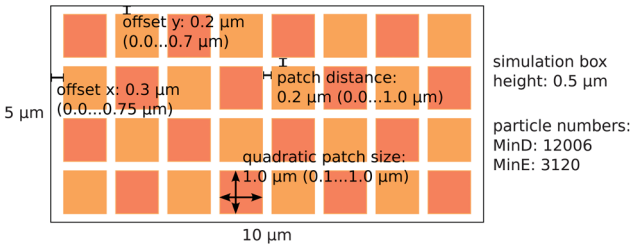

Fig. 2 Schematic view of the simulated geometry with exemplary data for patch size 1 µm and patch distance 0.2 µm. In the grid pattern all patches are present, whereas in the checkerboard pattern only the bright orange ones are present.

$$\mathrm{MinD-ADP + ATP} \xrightarrow{\lambda} \mathrm{MinD-ATP + ADP} \quad (1)$$

Only MinD–ATP is able to bind to the membrane. Membrane attachment of MinD–ATP can occur at any place with a fixed rate:

$$\mathrm{MinD-ATP} \xrightarrow{k_D} \mathrm{MinD(m)} \quad (2)$$

In the so-called cooperative attachment (CA) models MinD molecules preferentially bind to areas with high MinD concentrations on the membrane. To implement this in our model, we include the following reaction:

$$\mathrm{MinD(m) + MinD-ATP} \xrightarrow{k_{dD}} \mathrm{MinD(m) + MinD(m)} \quad (3)$$

MinD bound to the membrane can then bind a MinE molecule from the bulk, forming a MinDE complex bound to the membrane:

$$\mathrm{MinD(m) + MinE} \xrightarrow{k_{dE}} \mathrm{MinDE(m)} \quad (4)$$

MinE now hydrolyzes the ATP and subsequently both the MinD and the MinE molecules detach from the membrane:

$$\mathrm{MinDE(m)} \xrightarrow{k_{de}} \mathrm{MinD-ADP + MinE} \quad (5)$$

All molecules can diffuse both in the cytoplasm and the membrane as defined by the respective diffusion coefficients, which are D_D for cytosolic MinD, D_E for cytosolic MinE, D_d for membrane-bound MinD and D_{de} for membrane-bound MinDE. For our simulations here we use the parameters of the Huang-model.[21,23] We note that model parameters like λ or D might have different values in different experiments.[15,20,29] All parameters used in the simulations can be found in Table 1. As known from earlier studies, this leads to a typical pattern length scale of the Min-oscillations around 5 µm, like in cells.

2.2 Computer simulations

We performed our simulations in a rectangular box with dimensions 10 µm (major axis) × 5 µm (minor axis) × 0.5 µm (height) with reflective boundary conditions. The box dimensions were chosen such that the width corresponds to the length of a wildtype *E. coli* and that the length corresponds to the length of an *E. coli* cell that has grown to double the size without formation of a septum. Thus in principle oscillations along both axes could emerge, which will become important later. The lower surface of the simulation box is decorated with a pattern of quadratic patches that MinD can bind to, as shown in Fig. 2.

We use two kinds of patterns, a simple grid pattern as shown and a checkerboard pattern, where only the bright orange patches are present. The patch size is 0.1–1 µm and the patch distance is 0.1–1 µm (0–1 µm for the checkerboard pattern), both in steps of 0.1 µm. In order to avoid incomplete patches, we place the maximum pattern possible with complete patches in the center of the simulation box, leading to offsets both along the major axis and the minor axis. The particle numbers were chosen to be 12 006 for MinD (6003 MinD–ATP and 6003 MinD–ADP) and 3120 for MinE, which results in a comparable surface density to earlier experiments[30] and simulations.[22,23] At simulation start the particles were distributed randomly throughout the simulation box. Thus, every simulation run has an individual initial particle distribution. We performed our simulations with Smoldyn 2.28 which is a particle-based stochastic simulation tool for reaction-diffusion systems in user-defined geometries that is freely available at http://www.smoldyn.org.[28] This simulation framework has been successfully applied to many different biological systems, for example to protein diffusion between two electrofused cells.[31] Especially due to its versatility regarding geometries and reactions on 2D surfaces embedded in a 3D environment, it is very well suited for our purpose. It is similar to MCell in treating the volume as continuous, however, it is faster and the reactions are more accurate than with MCell.[28] The Smoldyn script files for all simulations shown here are available on request from the corresponding author. All simulations ran for 1200 s of simulated time with a time step of 10^{-4} s. This step size is a compromise between accuracy and reasonable simulation run times. For every single patch size/patch distance combination we ran five simulations. Smoldyn converts every reaction rate provided in the configuration script to either a probability (events per time step) for reactions of order 0 or 1 (reactions (1), (2), and (5)) or to a binding radius for reactions of order 2 (reactions (3) and (4)), which means that particles react once the distance between the two is smaller than the binding radius. This is necessary as the particles have no volume and, thus, cannot react *via* an encounter complex like in simulation tools explicitly modeling the volume of particles.[32,33] An interesting and less computer-time consuming alternative would be particle-based stochastic simulations with Green's Function

Reaction Dynamics (GFRD),[34,35] which however has difficulties in implementing non-trivial geometries.

2.3 Oscillation analysis

As we will see later, Min-oscillations show more complex spatiotemporal patterns than *e.g.* traveling waves and thus are not easily accessible by standard methods like Fourier analysis. Moreover we perform large-scale computer simulations and therefore need to use an automatic evaluation of large datasets. To this end, we have adopted the following method. We first compute the so-called *instantaneous oscillation period* T. From video sequences and kymographs of our simulations we find that oscillation periods vary from 10 s to 70 s. We therefore compute a correlation coefficient for time shifts in this window and then automatically identify the first maximum as T. This method was introduced in detail by Kerr *et al.*[22] We use MinD histograms for the window vectors with 2000 bins for the major axis and 1000 bins for the minor axis, taken every 0.1 s. For every simulation we computed the instantaneous oscillation period at $N = 375$ time points separately, both for potential oscillations along the major and the minor axis. These values have a well-defined average only if a stable oscillation pattern exists over the whole course of the simulation. In most cases, however, these values will vary widely, because no stable oscillation pattern exists or because the system is in a transition period between different states. Therefore the average of the instantaneous oscillation periods is not a good measure for our purpose.

To automatically detect oscillations and to analyze their dependence on patch size and patch distance, we instead introduce an *oscillation index* q that characterizes how well the oscillation period of a simulation agrees with the oscillation period of a reference simulation that showed oscillations. q is defined as

$$q = \frac{1}{N}\sum_{i=1}^{N} \mathrm{rect}\left(\frac{T_i - \overline{T}}{2\sigma}\right). \quad (6)$$

T_i is the i-th instantaneous oscillation period of the $N = 375$ values determined during a simulation run. $\overline{T}$ is a reference oscillation period. Our standard choice will be $\overline{T} = 33.6$ s, which is the average value measured in simulations with a homogeneous substrate. However, as will be shown below, this value can be adapted to special situations when needed. rect is the rectangular function. σ is a measure of the allowed deviation of the instantaneous oscillation period from the average oscillation period in order to still be counted. Again based on simulations for homogeneous substrates, we set $\sigma = 3$ s. This is in line with the results by Kerr *et al.*[22] that showed a deviation of about 6–7 s at oscillation periods roughly twice as long as ours. Below we will evaluate q either for one of the two axes separately or we will take the average of the two values.

3 Results

3.1 Two different oscillation patterns on a homogeneous substrate

We first analyze the oscillations emerging if MinD–ATP attaches homogeneously to the substrate as a reference case for the later analysis on patterns. In Fig. 3 we show two examples of our simulations, which emerged spontaneously for the same parameter sets due to small differences in the initial conditions. The kymograph gives a two-dimensional representation of the spatiotemporal development of a system. For every time point (horizontal axis) the corresponding histogram is plotted along the vertical axis. In the kymographs the sum of MinD and MinDE is plotted. The resolution is 1 s along the time axis and 0.05 μm along the position axis. The left example shows striped oscillations along the major axis, whereas the right example shows pole-to-pole oscillations along the minor axis. For a better understanding of the difference between these two patterns, we show two series of simulation snapshots in the ESI (Fig. S1†). Note that both patterns are quite different from simple wave propagation and consist of spatiotemporal cycles of localization and delocalization of the Min-proteins on certain regions of the membrane. Due to the small system size we observe neither spiral patterns nor diagonal oscillations. The emergence of oscillations along the minor axis seems at odds with the observation that Min-oscillations in wildtype *E. coli* cells always have the major axis as the main oscillation axis. However, in our simulations this typical pattern length scale fits the length of the minor axis. We find almost identical results for the mean oscillation period for both oscillation patterns (striped oscillations: 33.68 s, pole-to-pole oscillations: 33.51 s), which are well in line with published results for similar parameter sets.[21,23] In summary, our stochastic approach in combination with the chosen geometry allows us to identify two different oscillation patterns which emerge stochastically due to small differences in the initial conditions. This shows the strength of the stochastic simulation approach, because such a finding cannot easily be obtained with a PDE-approach.

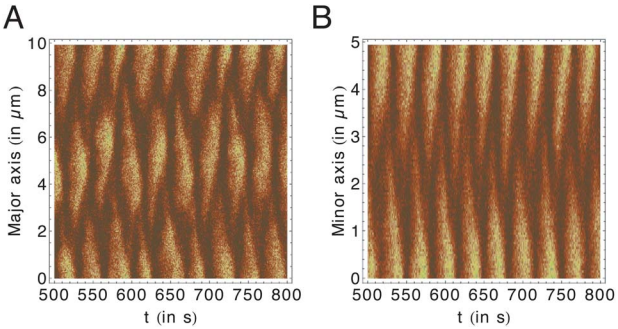

Fig. 3 Kymographs of two different simulations with a homogeneous substrate at the bottom of the box. The first sample (A) shows striped oscillations along the major axis, whereas the second sample (B) shows pole-to-pole oscillations along the minor axis. Both simulations have the same parameters, but spontaneously develop different stable oscillation patterns from slightly different initial particle positions.

3.2 Switch between oscillation patterns triggered by patch geometry

After verifying our approach with some reference simulations, we next illustrate a surprising effect one finds on patches. Later we analyze it in more detail with a complete set of simulations. In Fig. 4A and B we show typical kymographs for oscillations

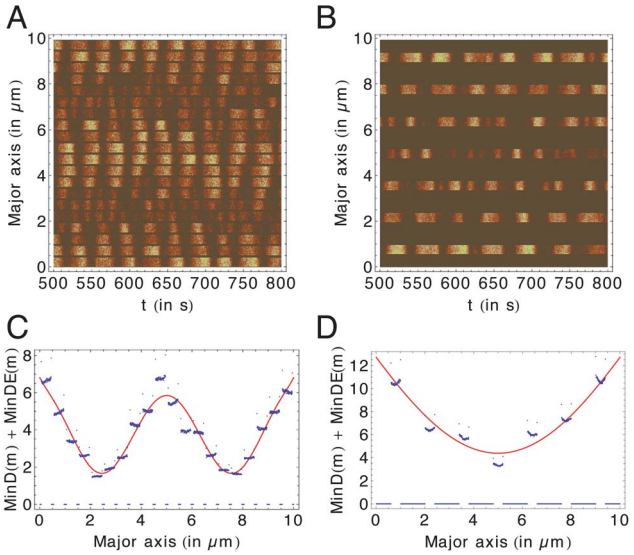

Fig. 4 Kymographs along the major axis of the combined membrane-bound MinD and MinDE concentration for the grid pattern for simulations with patch size 0.4 μm and (A) patch distance 0.1 μm and (B) patch distance 1.0 μm. For the small patch distance perfectly striped oscillations are visible with a period of about 30–35 s. For the large patch distance this surprisingly changes to a pole-to-pole oscillation pattern with an oscillation period of about 45 s. To highlight the nature of the different oscillation patterns we also show the corresponding time-averaged histograms (C and D) below. The red lines are guides to the eye and have been obtained by polynomial fitting. The data points have slightly higher values at the end of each patch due to the handling of surface-bound particles at the edges of surfaces in Smoldyn and the very small bin size.

along the major axis on the grid pattern with patch size 0.4 μm. For small patch distances (Fig. 4A) the expected striped pattern comparable to filamentous cells arises. This shows that Min-oscillations are sufficiently robust to tolerate small perturbations in the substrate. Surprisingly, however, for larger patch distances (Fig. 4B), we typically find pole-to-pole oscillations arising along the major axis (ESI, Movie S2†). Fig. 4C and D are time-averaged histograms demonstrating the different nature of the two observed oscillation patterns. The observed switching between them is especially interesting as previously a change in the intrinsic pattern length scale was discussed to depend on the parameter values used.[20] Here, however, we did not change any parameter, but the patch geometry. This change in the oscillation pattern is also coupled to an increase of the oscillation period from about 30 s to about 45 s. This is very different from the effect of temperature variations that change the oscillation period but not the typical pattern length scale.[36] We will discuss this change in the oscillatory pattern in detail in Section 3.4, especially regarding a possible dependence on the chosen patch size/patch distance combination.

3.3 Stochastic switching between different oscillation patterns

Our special choice of the simulation geometry allows oscillations in both directions and indeed we find stochastic switching between the different oscillation patterns. A typical example for this can be seen in Fig. 5, in which we show kymographs for one

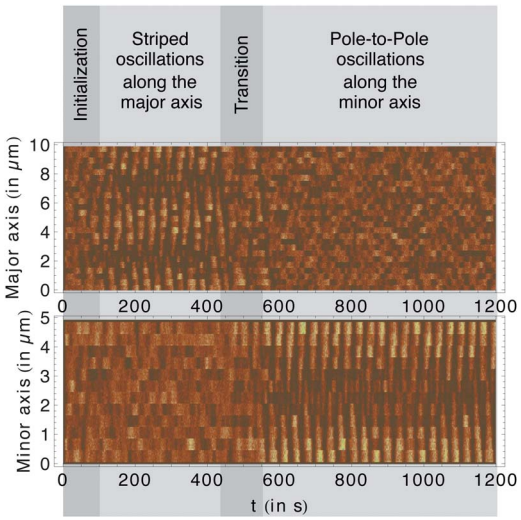

Fig. 5 Kymographs along the major (upper kymograph) and the minor axis (lower kymograph) of the combined membrane-bound MinD and MinDE concentration for the same simulation run with the checkerboard pattern with patch size 0.4 μm and patch distance 0 μm. After the initialization phase (t < 100 s) striped oscillations along the major axis emerge. However, due to stochastic fluctuations this oscillation pattern switches to a pole-to pole oscillation pattern along the minor axis with a transition period in between of about 100 s.

simulation run with the checkerboard pattern with patch size 0.4 μm and patch distance 0 μm. After the usual initialization period, for times below 450 s there is an oscillation along the major axis. Due to stochastic fluctuations, the stable oscillations along the major axis switch to pole-to-pole oscillations (t > 550 s) with quite a long transition period of about 100 s in between. This switch can also be nicely observed in a movie of the simulation (ESI, Movie S3†). We have noticed this switching behavior for numerous samples, indicating that there is apparently no preferred oscillation axis, which is important for the oscillation analysis in the next section. Like for the reference simulations on the homogeneous substrate, it should be noted that the oscillation period along the minor axis is similar to the one along the major axis (around 30–35 s), as can be seen by comparing the kymographs.

If the patch distance is increased to 1.0 μm, in contrast to the grid pattern there are no stable oscillations any more on the checkerboard pattern along either axis (data not shown). This suggests that there might exist a critical patch distance. Above this patch distance no oscillations arise like those found for the checkerboard pattern; alternatively they show a different oscillation pattern as observed for the grid pattern. The existence of a critical patch distance raises two interesting questions. First, is this patch distance fixed for all patch sizes or is there any correlation? Second, is there any difference between the grid and the checkerboard pattern as our two examples shown suggest? To tackle these questions, we performed an in-depth oscillation analysis of the instantaneous oscillation periods.

3.4 Results of the automatic oscillation analysis

3.4.1 Oscillations along both axes are patch size and patch distance dependent. As shown in Fig. S4,† the instantaneous

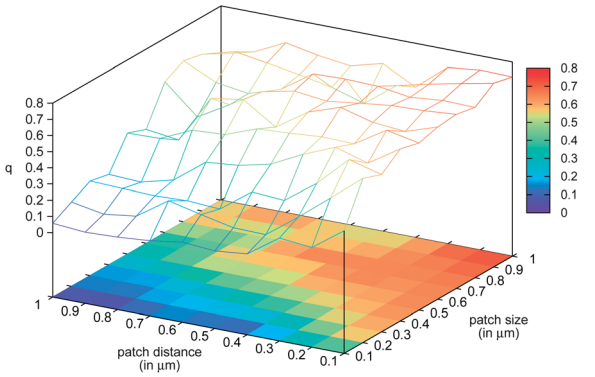

Fig. 6 3D and 2D plot of the oscillation index q for $\bar{T} = (33.6 \pm 3)$ s for oscillations along both the major and the minor axis (average value) depending on the patch size and patch distance for the grid pattern. The plot highlights the sharp boundary between patch size/patch distance combinations with and without oscillations.

oscillation periods vary widely during a typical computer simulation and we therefore use the oscillation index q to automatically detect the presence of an oscillation with a period around a given reference value. We start our analysis with the grid pattern. In Fig. 6 we show the results for the automatically measured oscillation index q for the different patch sizes and distances. The data points are shown as a 3D grid and as a 2D density plot with each tile colored according to the mean value of the four corner points. The results shown are the combined results for the major and minor axes (average value). Two features are important to note: first, there is a clear dependence on the patch distance that is however coupled to the patch size. For increasing patch size the distance between neighboring patches can be much larger for stable oscillations. Second, the combined analysis still yields q of up to 0.7, which means that 70% of all measurements yielded oscillation periods within 3 s of the reference oscillation period. With q being over 0.5 (which would be the case for perfect oscillations along one axis and no matching instantaneous oscillation period along the other axis) there must exist oscillations along the apparently non-oscillating axis. These can either come from long transition periods during axis switching or are present but not visible due to being overlaid by the dominant oscillation along the other axis. The q-values for the largest patch sizes with the smallest patch distances are well in line with the results for the oscillations on the homogeneous substrate, which yielded $q \approx 0.72$. $q = 1$ would mean simultaneous perfect oscillations along both the major and the minor axes and we have never observed this to occur. We also mention that the data for the individual axis (major and minor) look very similar (see Fig. S5†), which indicates that there is no preferential oscillation direction for a given geometry.

For the checkerboard pattern the results shown in Fig. 7 are qualitatively similar with regard to the patch size dependence. There is one major quantitative difference, though, the oscillations vanish for noticeably smaller patch distances compared to the grid pattern. However, we note that q would be significantly higher in those regions if one scans for oscillations with $27.6\ \text{s} < t < 36.6\ \text{s}$.

3.4.2 Emergence of pole-to-pole oscillations. Probably the most intriguing feature unveiled by our simulations above was the tendency for pole-to-pole oscillations along the major axis to emerge instead of the expected striped pattern. As apparently the oscillation periods were longer (see Fig. 4), we reanalyzed the oscillation periods with a reference oscillation period of $\bar{T} = 46$ s while keeping the allowed deviations constant at $\sigma = 3$ s. The choice of the mean oscillation period was made based on selected kymographs from our simulations.

We start with the grid pattern. As the change in oscillation behavior only occurs for oscillations along the major axis but not along the minor axis, we will treat them separately. For the major axis along which the pole-to-pole oscillations were noticed the results are shown in Fig. 8. In line with our expectations from our simulation results, there is a sharp ridge with maxima of q around 0.4 in the 3D plot which roughly runs along the boundary between areas in the plot with high and with low q. This confirms that for these combinations of patch size and distance, the system switches to pole-to-pole oscillations with a longer oscillation period and the above shown samples are

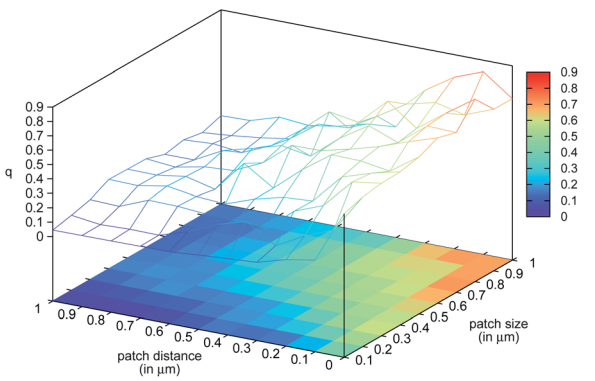

Fig. 7 Same as in Fig. 6 but for the checkerboard pattern. In general the result is comparable, note however that for larger patch sizes there are no oscillations emerging for large patch distances.

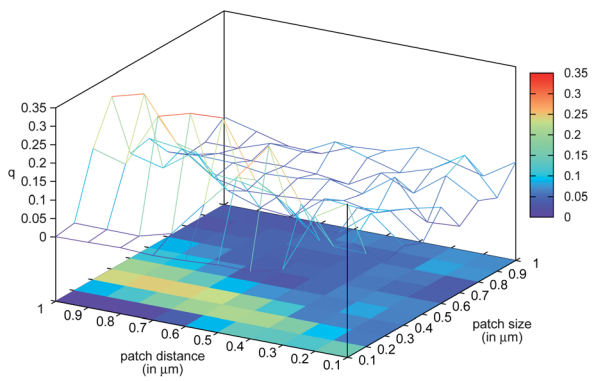

Fig. 8 3D and 2D plot of q for oscillations with an oscillation period of (46 ± 3) s along the major axis depending on the patch size and patch distance for the grid pattern. A clear ridge rises along the boundary of geometries with or without oscillations, indicating the presence of pole-to-pole oscillations along the major axis for these geometries.

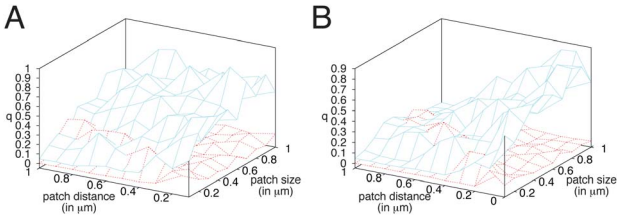

Fig. 9 Overlay of the data for q for oscillations with a period of $T = (33.6 \pm 3)$ s (cyan) and a period of $T = (46 \pm 3)$ s (red) along the major axis for the grid pattern (A) and the checkerboard pattern (B). The plots highlight the patch size and patch distance combinations where pole-to-pole oscillations dominate.

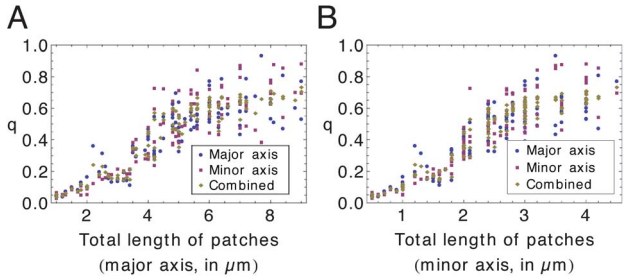

Fig. 10 Dependence of q for $\bar{T} = (33.6 \pm 3)$ s on the total length of the patches for the grid pattern along the major axis (A) and the minor axis (B). Note that both plots level out.

indeed typical of the oscillation patterns arising. In sharp contrast to that, there is no such increase for the oscillations along the minor axis (see Fig. S6†). The maximum q value is roughly $q \approx 0.1$ with the peaks being distributed all over the patch size/patch distance space, indicating that these peaks are most probably due to stochastic fluctuations and not due to any geometrical effects.

For the checkerboard pattern the results are again very similar (see Fig. S7†) apart from the ridge running more diagonal in the patch size/patch distance plane in comparison to the grid pattern. This is in line with the results for the normal oscillations that also had a much more diagonal running boundary between areas with high and low q (see Fig. 7). Again there are no significant increases for the results along the minor axis, underlining the fact that this switch of oscillation pattern is happening solely along the major axis but not along the minor axis. The latter is however not too surprising as due to the shorter length only pole-to-pole oscillations are possible. We note that the exact results may differ by varying $\bar{T}$ and or σ. For example, some of the examples shown above have indicated oscillation periods over 50 s. However, even with a detection window of 44–60 s, no qualitative changes to the results shown can be noted.

For a better comparison, in Fig. 9 we show an overlay of the results for $\bar{T} = 33.6$ s (cyan) and $\bar{T} = 46$ s (red). For both, the grid pattern (left panel) and the checkerboard pattern (right panel), it can be seen that for oscillations along the major axis the pole-to-pole oscillations – for those patch size/patch distance combinations where they occur – are present even slightly more than oscillation periods hinting at striped oscillations. As noted above the pole-to-pole oscillations are bracketing the areas with a high occurrence of striped oscillations.

3.4.3 Effect of the total length of patches. In the literature the transition from pole-to-pole patterns to striped patterns has always been linked to a growing cell length[2,15,23,36] for constant parameters. To the best of our knowledge only one publication[37] mentions a switch from striped patterns to pole-to-pole oscillations without variations in cell length, although in this case, the pole-to-pole oscillations are not as distinct as in our simulations with up to a decade longer oscillation periods and the model is one-dimensional. Recently Halatek and Frey[20] showed that striped oscillations can emerge out of pole-to-pole oscillations for cells of length 12 μm, however only if MinD recruitment was fast enough to strengthen weak polar zones. Based on this reported length dependence, we wanted to identify any effect that our specific simulation geometries might have on the oscillation behavior. Two possible length scales may play a role: due to the distances between the patches the actual length of MinD binding patches is much shorter than the simulation box, but also the total length of the pattern including the gaps is shorter due to the offsets at both sides (see Fig. 2).

For the total pattern length we found no significant dependence of q on the total pattern length except for slightly lower q values for the shortest checkerboard pattern lengths (see Fig. S8†). This also holds true if we plot the data for q for a reference oscillation period of $\bar{T} = (46 \pm 3)$ s (see Fig. S9†). Thus, the emerging pole-to-pole oscillations are not due to a shorter total pattern length compared to the other samples. To check for any dependencies of the oscillations on the total length of the patches (meaning the number of patches in one row (grid pattern) or in two adjacent rows (checkerboard pattern) along the major or minor axis times the size of a patch), we plotted q against the total length of the patches for the grid pattern in Fig. 10 and for the checkerboard pattern in Fig. S10.† From both figures it becomes clear that indeed q is dependent on the total length of the patches, which is not too surprising as a small length of patches means very large distances, which were shown to break oscillation patterns above. However, this effect seems to level out for both geometries, albeit at a lower total patch length in the grid than in the checkerboard pattern. This result is in line with the above results that on the checkerboard pattern the oscillations vanish for lower patch distances at the same patch size.

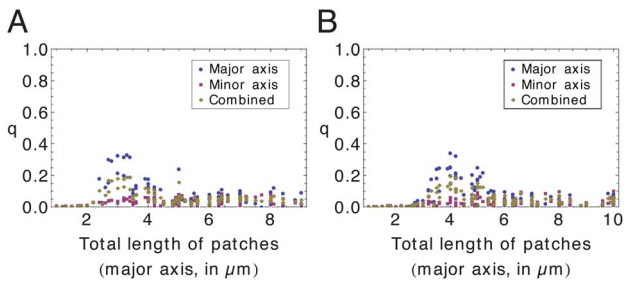

Fig. 11 Dependence of q for $\bar{T} = (46 \pm 3)$ s on the total length of the patches for the grid pattern along the major axis for the grid pattern (A) and the checkerboard pattern (B). Note the clustering of samples with large q values around total patch lengths of 2–5 μm.

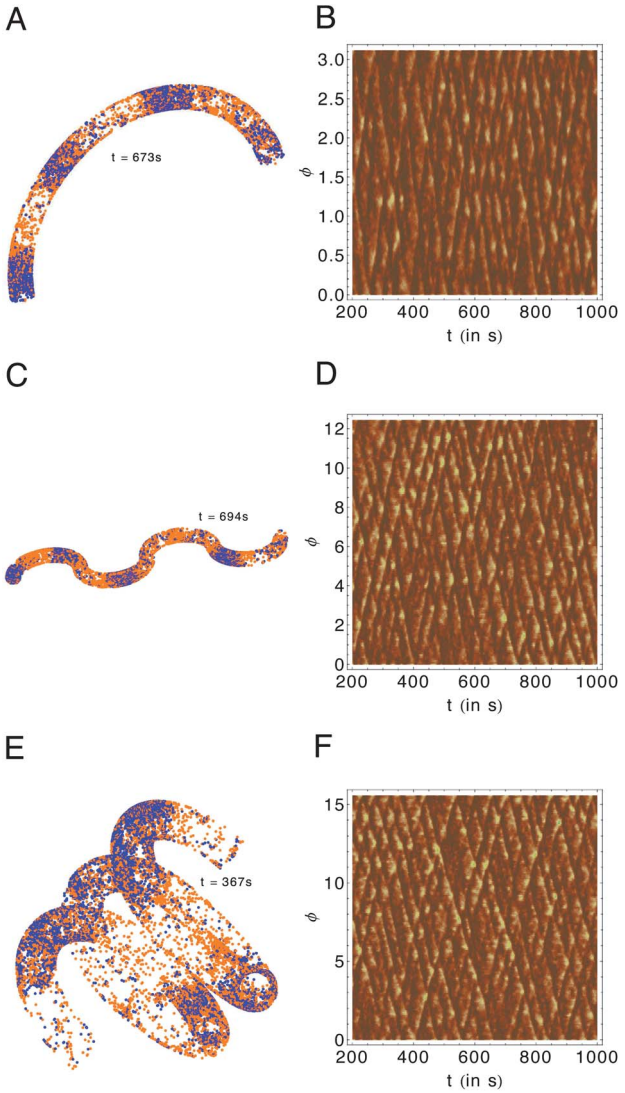

Fig. 12 Min oscillations in crescent- (A and B), sinusoidal- (C and D), and helix-shaped (E and F) *E. coli* cells. The screenshots show an oscillation behavior similar to the filamentous cells. Membrane-bound MinD is marked in blue and membrane-bound MinDE is marked in orange. Due to the much longer cells there are more nodes. The number of nodes increases with increasing cell length. This is underlined by the kymographs in the right panel. ϕ marks the position along the cell contour.

As our focus is on the occurrence of the pole-to-pole oscillations along the major axis, we perform the same analysis but for a q calculated for a mean oscillation period of $\bar{T} = (46 \pm 3)$ s. The results are shown in Fig. 11 for both, the grid pattern (left panel) and the checkerboard pattern (right panel). Here it is very interesting that both graphs peak for values between 2 μm and 5 μm with the peak slightly shifted to larger values for the checkerboard pattern. These total patch lengths are all of the size of a wildtype *E. coli* cell that shows rod-like oscillations, which might lead to the conclusion that this is the reason why these patterns are producing pole-to-pole instead of striped oscillations. However, there are also oscillations with the shorter, expected oscillation period with very similar q-values at these total patch lengths.

3.5 Exploring three dimensions

In our simulations we have shown the variety in oscillation patterns on a 2D patterned substrate. Using Smoldyn as the simulation software we envision taking this approach further by simulating patterned structures also in more complex geometries which make full use of the three dimensions. As instructive examples for three-dimensional geometries, we turn to the crescent-, sinusoidal-, and helix-shaped *E. coli* cells, which have been grown by Takeuchi *et al.*[38] In Fig. 12 we show a screenshot and a kymograph of a reference simulation for each of these geometries. A movie of the simulation of the helix-cell can be found in the ESI (Movie S11†). ϕ denotes the angle marking the position along the cell. The crescent-shaped cell has a total length of 39.6 μm, and the sinusoidal-shaped cell is about 62.8 μm long. The diameter of the helix is approximately 10 μm, leading to a total cell length of about 78.5 μm. For these simulations k_D was set to 0.0125 μm s^{-1}, all other parameters remained the same. The particle numbers were increased to reflect the longer cell lengths. Very similar to the filamentous *E. coli* cells, we observe striped patterns with an increasing number of nodes due to the increasing cell length from the crescent- to the helix-shaped cell. For all three shapes the typical pattern length scale and the periods of the oscillations are roughly comparable to those on the homogeneous substrate.

4 Conclusions

In this paper we have demonstrated that investigating Min-oscillations on micropatterns with typical patch sizes being small compared to the typical pattern length scale of the oscillations leads to very interesting results. We first confirm that Min-oscillations are sufficiently robust as to tolerate small gaps in the substrate. We next find that there exists a patch distance above which no stable oscillations can be recorded, in agreement with results for larger patterns.[16] However, it has not been shown before how patch size and distance have to be chosen to still ensure the emergence of oscillations. In our chosen geometry the main oscillation axis can be oriented either along the major or the minor axis with stochastic switches between different oscillation patterns, underlining the need to include stochasticity in such simulations. Our most striking result in regard to the effect of geometry is the finding that the system can also be switched between different oscillation patterns along the same oscillation axis by changing patch geometry only. Until now, such a switch has only been observed through changes in system size (switch from pole-to-pole to striped by increasing cell length).

Our approach provides a powerful framework to understand the effects of three dimensions, stochasticity and geometry on Min-oscillations, both in living cells and in reconstitution assays. For example, the unusual three-dimensional cell shapes produced by Takeuchi and coworkers[38] could also be engineered and patterned in suitable material systems. Regarding the important biological system of the *E. coli* cells, our results suggest that small variations in putative division sites are not sufficient to change the character of the Min-oscillations. On

the other hand, however, a cell-scale distribution of such sites might in fact switch the oscillation pattern. This might be an important element to understand, *e.g.* the division of certain nematode-attached gammaproteobacteria from the family Chromatiaceae.[39] In contrast to *E. coli* cells, these ecto-symbionts divide along the long rather than along the short axis. The evolutionary advantage of this unusual process seems to be the fact that these gammaproteobacteria are attached with one pole to the surface of the marine nematode *Laxus oneistus* and thus have to make sure that both daughter cells remain attached to the host after division.[40] It is an exciting question to explore if internal patterning of division sites might in fact lead to Min-oscillations along the short axis of the bacterium.

Acknowledgements

This work was supported by the BMBF-program MechanoSys (grant number 0315501C). USS is a member of the Heidelberg cluster of excellence CellNetworks. We thank Steve Andrews for helpful discussions regarding Smoldyn.

References

1 P. A. de Boer, R. E. Crossley and L. I. Rothfield, *Cell*, 1989, **56**, 641–649.
2 D. M. Raskin and P. A. J. de Boer, *Proc. Natl. Acad. Sci. U. S. A.*, 1999, **96**, 4971–4976.
3 Z. Hu and J. Lutkenhaus, *Mol. Microbiol.*, 1999, **34**, 82–90.
4 P. A. de Boer, R. E. Crossley and L. I. Rothfield, *J. Bacteriol.*, 1992, **174**, 63–70.
5 E. Bi and J. Lutkenhaus, *Nature*, 1991, **354**, 161–164.
6 J. Lutkenhaus, *Annu. Rev. Biochem.*, 2007, **76**, 539–562.
7 P. Lenz and L. Søgaard Andersen, *Nat. Rev. Microbiol.*, 2011, **9**, 565–577.
8 M. Loose, K. Kruse and P. Schwille, *Annu. Rev. Biophys.*, 2011, **40**, 315–336.
9 V. Ivanov and K. Mizuuchi, *Proc. Natl. Acad. Sci. U. S. A.*, 2010, **107**, 8071–8078.
10 B. Di Ventura and V. Sourjik, *Mol. Syst. Biol.*, 2011, **7**, 457.
11 A. Varma, K. C. Huang and K. D. Young, *J. Bacteriol.*, 2008, **190**, 2106–2117.
12 B. D. Corbin, X.-C. Yu and W. Margolin, *EMBO J.*, 2002, **21**, 1998–2008.
13 J. Männik, F. Wu, F. J. H. Hol, P. Bisicchia, D. J. Sherratt, J. E. Keymer and C. Dekker, *Proc. Natl. Acad. Sci. U. S. A.*, 2012, **109**, 6957–6962.
14 M. Loose, E. Fischer-Friedrich, J. Ries, K. Kruse and P. Schwille, *Science*, 2008, **320**, 789–792.
15 M. Loose, E. Fischer-Friedrich, C. Herold, K. Kruse and P. Schwille, *Nat. Struct. Mol. Biol.*, 2011, **18**, 577–583.
16 J. Schweizer, M. Loose, M. Bonny, K. Kruse, I. Mönch and P. Schwille, *Proc. Natl. Acad. Sci. U. S. A.*, 2012, **109**, 15283–15288.
17 H. Meinhardt and P. A. de Boer, *Proc. Natl. Acad. Sci. U. S. A.*, 2001, **98**, 14202–14207.
18 M. Howard, A. Rutenberg and S. de Vet, *Phys. Rev. Lett.*, 2001, **87**, 278102.
19 K. Kruse, *Biophys. J.*, 2002, **82**, 618–627.
20 J. Halatek and E. Frey, *Cell Rep.*, 2012, **1**, 741–752.
21 K. C. Huang, Y. Meir and N. S. Wingreen, *Proc. Natl. Acad. Sci. U. S. A.*, 2003, **100**, 12724–12728.
22 R. A. Kerr, H. Levine, T. J. Sejnowski and W.-J. Rappel, *Proc. Natl. Acad. Sci. U. S. A.*, 2006, **103**, 347–352.
23 D. Fange and J. Elf, *PLoS Comput. Biol.*, 2006, **2**, e80.
24 K. Kruse, M. Howard and W. Margolin, *Mol. Microbiol.*, 2007, **63**, 1279–1284.
25 K.-T. Park, W. Wu, K. P. Battaile, S. Lovell, T. Holyoak and J. Lutkenhaus, *Cell*, 2011, **146**, 396–407.
26 N. Pavin, H. Paljetak and V. Krstić, *Phys. Rev. E: Stat., Nonlinear, Soft Matter Phys.*, 2006, **73**, 021904.
27 S. S. Andrews and D. Bray, *Phys. Biol.*, 2004, **1**, 137–151.
28 S. S. Andrews, N. J. Addy, R. Brent and A. P. Arkin, *PLoS Comput. Biol.*, 2010, **6**, e1000705.
29 G. Meacci, J. Ries, E. Fischer-Friedrich, N. Kahya, P. Schwille and K. Kruse, *Phys. Biol.*, 2006, **3**, 255–263.
30 Y.-L. Shih, I. Kawagishi and L. Rothfield, *Mol. Microbiol.*, 2005, **58**, 917–928.
31 G. Gerisch, M. Ecke, R. Neujahr, J. Prassler, A. Stengl, M. Hoffmann, U. S. Schwarz and E. Neumann, *J. Cell Sci.*, 2013, **126**, 2069–2078.
32 J. Schluttig, D. Alamanova, V. Helms and U. S. Schwarz, *J. Chem. Phys.*, 2008, **129**, 155106.
33 J. E. Baschek, H. C. R. Klein and U. S. Schwarz, *BMC Biophys.*, 2012, **5**, 22.
34 J. van Zon and P. ten Wolde, *Phys. Rev. Lett.*, 2005, **94**, 128103.
35 K. Takahashi, S. Tanase-Nicola and P. R. ten Wolde, *Proc. Natl. Acad. Sci. U. S. A.*, 2010, **107**, 2473–2478.
36 A. Touhami, M. Jericho and A. D. Rutenberg, *J. Bacteriol.*, 2006, **188**, 7661–7667.
37 F. Tostevin and M. Howard, *Phys. Biol.*, 2006, **3**, 1–12.
38 S. Takeuchi, W. R. DiLuzio, D. B. Weibel and G. M. Whitesides, *Nano Lett.*, 2005, **5**, 1819–1823.
39 N. Leisch, J. Verheul, N. R. Heindl, H. R. Gruber-Vodicka, N. Pende and T. D. Blaauwen, *Curr. Biol.*, 2012, **22**, R831–R832.
40 M. F. Polz, H. Felbeck, R. Novak, M. Nebelsick and J. A. Ott, *Microb. Ecol.*, 1992, **24**, 313–329.

